

Study of the exclusive reaction $pp \rightarrow ppK^{*0}\bar{K}^{*0}$: $f_2(1950)$ resonance versus diffractive continuum

Piotr Lebiedowicz^{1,*}

¹*Institute of Nuclear Physics Polish Academy of Sciences,
Radzikowskiego 152, PL-31342 Kraków, Poland*

Abstract

We present first predictions of the cross sections and differential distributions for the exclusive reaction $pp \rightarrow ppK^{*0}\bar{K}^{*0}$ contributing to the $K^+K^-\pi^+\pi^-$ channel. The amplitudes for the reaction are formulated within the nonperturbative tensor-pomeron approach. We consider separately the $f_2(1950)$ s -channel exchange mechanism and the K^{*0} t/u -channel exchange mechanism, focusing on their specificities. First mechanism is a candidate for the central diffractive production of tensor glueball and the second one is an irreducible continuum. We adjust parameters of our model, assuming the dominance of pomeron-pomeron fusion, to the WA102 experimental data. We find that including the continuum contribution alone one can describe the WA102 data reasonably well. We present predictions for the reaction $pp \rightarrow pp(K^{*0}\bar{K}^{*0} \rightarrow K^+K^-\pi^+\pi^-)$ for the ALICE, ATLAS, CMS and LHCb experiments including typical kinematical cuts. We find from our model a cross sections of $\sigma \cong 17 - 250$ nb for the LHC experiments, depending on the assumed cuts. Absorption effects are included in our analysis.

*Electronic address: Piotr.Lebiedowicz@ifj.edu.pl

I. INTRODUCTION

Studies of the $K^*\bar{K}^*$ system have been carried out in two-photon interactions [1–3], in radiative J/ψ decay [4, 5], in $K^-p \rightarrow K^*\bar{K}^*\Lambda$ reaction [6, 7], and in central production in proton-proton collisions [8–10]. It is known from the WA102 experiment [10] that although the $K^{*0}\bar{K}^{*0}$ final state is a major component of the $K^+K^-\pi^+\pi^-$ channel it is not the dominant component. In contrast, the $\phi\phi$ final state was found to be dominant component of the $K^+K^-K^+K^-$ channel [11]. The cross section as a function of center-of-mass energy for the production of $K^*(892)\bar{K}^*(892)$ system was found [10] to be consistent with being produced via the double-pomeron-exchange mechanism.

In hadronic proton-proton collisions [9, 10, 12] a broad low-mass enhancement in the $K^*\bar{K}^*$ and/or $K^+K^-\pi^+\pi^-$ invariant mass distributions was seen. In [9] the authors stated that the $K^{*0}\bar{K}^{*0}$ system is mainly produced as a nonresonant threshold enhancement. More recent analysis [13] give some evidence for the existence of $f_2(1950)$ resonance in the $K^{*0}\bar{K}^{*0}$ channel; see Fig. 3 (c) of [13]. On the other hand, in the radiative J/ψ decay [4, 5] the $K^*\bar{K}^*$ spectrum indicates two narrow peaks at low mass. The analysis of angular distributions finds that the $K^*\bar{K}^*$ system in the radiative J/ψ decay show strong $J^{PC} = 0^{-+}$ component whereas the hadronic production modes are all consistent with strong (broad) $J^{PC} = 2^{++}$ component. The analysis of the partial wave structure of the $K^{*0}\bar{K}^{*0}$ state from the reaction $\gamma\gamma \rightarrow K^+K^-\pi^+\pi^-$ [3] support the dominance of the $(J^P, J_z) = (2^+, \pm 2)$ wave.

An interesting suggestion has been made for the broad isoscalar-tensor $f_2(1950)$ resonance to be the lightest tensor glueball, while the arguments are not yet fully settled. Namely, this state is occasionally discussed as a candidate for a tensor glueball as it appears to have largely flavor-blind decay modes; see e.g. [14–16]. However, according to lattice-QCD simulations, the lightest tensor glueball has a mass between 2.2 GeV and 2.4 GeV, see, e.g., [17–19]. Thus, the $f_2(2300)$ and $f_2(2340)$ states are good candidates to be tensor glueball. The nature of these resonances is not understood at present and a tensor glueball has still not been clearly identified. Nontrivial are predictions of not only masses but also widths of the predicted glueballs; see, e.g., Sec. 8 of [20] for more information on this topic. Glueballs are expected to lie on the pomeron trajectory. It was shown in [20] that even small variations of the parameters in the (nonlinear) pomeron/glueball trajectory result in noticeable changes of glueballs widths.

It is also interesting to speculate whether the tensor states $f_2(1910)$, $f_2(1950)$, and $f_2(2150)$, observed by the WA102 Collaboration [21], are due to mixing between a tensor glueball and nearby $q\bar{q}$ states. Two of these states have similar ϕ_{pp} and dP_t dependencies and one the opposite; ϕ_{pp} is the azimuthal angle between the transverse momentum vectors of the outgoing protons, and dP_t is the so-called “glueball-filter variable” [22] defined by the difference of the transverse momentum vectors of the outgoing protons. It is known from the WA102 analysis of various channels that all the undisputed $q\bar{q}$ states are suppressed at small dP_t in contrast to glueball candidates. Established $q\bar{q}$ states peak at $\phi_{pp} = \pi$ whereas the $f_2(1910)$ and $f_2(1950)$ peak at $\phi_{pp} = 0$ [21]. These experimental observations in central production indicate that the $f_2(1950)$ probably contains large gluonic component and should be copiously produced via the double-pomeron-exchange (i.e., PP-fusion) mechanism.

However, the observation of $f_2(1950)$ resonance in two-photon interaction processes, such as $\gamma\gamma \rightarrow f_2(1950) \rightarrow K^{*0}\bar{K}^{*0}$ [1–3], and in other $\gamma\gamma$ -fusion processes [23–25], pre-

cludes its interpretation as a pure gluonic state. In [25] a good description the Belle data on $\gamma\gamma \rightarrow p\bar{p}$ including, in addition to the proton exchange, the $f_2(1950)$ resonance was obtained. One can observe there the dominance of the $f_2(1950)$ resonance in the low mass region $M_{p\bar{p}} = W_{\gamma\gamma} < 2.5$ GeV. In the $f_2(1950)$ -exchange amplitude only the term with $a_{f_2(1950)\gamma\gamma}$ coupling and $g_{f_2(1950)p\bar{p}}^{(2)}$ coupling was used. There, a - and b -type coupling parametrise the so-called helicity-zero and helicity-two $\gamma\gamma \rightarrow f_2$ amplitudes, respectively; see e.g. [26]. For instance, for the $\gamma\gamma \rightarrow f_2(1270)$ process the helicity-2 contribution (b -type coupling) is dominant. As will be presented in this work, for diffractive processes shown in Fig. 1, the b -type coupling in the $f_2(1950)K^{*0}\bar{K}^{*0}$ and $\mathbb{P}K^*K^*$ vertices is more preferred than the a -type coupling.

The study of $\phi\phi$ and $K^*\bar{K}^*$ systems could provide also helpful information for searching for the fully-strange ($ss\bar{s}\bar{s}$) tetraquark. In the relativistic quark model based on the quasipotential approach in QCD [27], the $f_2(1950)$ and $f_2(2340)$ states are considered as a candidates for the ground state ($\langle L^2 \rangle = 0$) light tetraquarks as diquark-antidiquark (composed from an axial vector diquark and antidiquark), $qq\bar{q}\bar{q}$ and $ss\bar{s}\bar{s}$, respectively. In [28] the $f_2(2300)$ is assigned to be $ss\bar{s}\bar{s}$ tetraquark state. These two states $f_2(2300)$ and $f_2(2340)$ are close in mass within errors [29]. Very recently, in [30] it was stated that the $f_2(2340)$ resonance may be assigned to 1S-wave tetraquark $T_{ss\bar{s}\bar{s}}(2381)$ in the framework of a nonrelativistic potential quark model without the diquark-antidiquark approximation. The $f_2(2340)$ state may have large decay rates into the $\phi\phi$ and $\eta\eta$ final states through quark rearrangements, and/or into $K^*\bar{K}^*$ final state through the annihilation of $s\bar{s}$ and creation of a pair of nonstrange $q\bar{q}$. To confirm this assignment, the above decay modes and such as $\eta\eta'$, $\eta'\eta'$ should be investigated in experimental searches. On the other hand, flavor mixings could be important for the light flavor systems and pure $ss\bar{s}\bar{s}$ states may not exist; see, e.g., [31].

With the idea of bringing more information on the topic, in the present work, we study the diffractive $\mathbb{P}\mathbb{P} \rightarrow f_2(1950)$ fusion mechanism in the reaction $pp \rightarrow ppK^{*0}\bar{K}^{*0}$ and the $K^{*0}\bar{K}^{*0}$ continuum which is a background for diffractively produced resonances. But we emphasize that in the following we make no assumptions on whether the $f_2(1950)$ resonance is glueball or tetraquark. The problem is interesting because of the production of expected glueballs can be associated with other mesons and can be accompanied by a diffractive continuum making the identification of glueballs rather difficult.

In the tensor-pomeron model for soft high-energy scattering formulated in [26], on the basis of earlier work [32], the pomeron exchange is effectively treated as the exchange of a rank-2 symmetric tensor. In the last few years a scientific program was undertaken to analyse the central exclusive production of mesons in the tensor-pomeron model in several reactions: $pp \rightarrow ppM$ [33], where M stands for a scalar or pseudoscalar meson, $pp \rightarrow pp\pi^+\pi^-$ and $pp \rightarrow pp(f_2(1270) \rightarrow \pi^+\pi^-)$ [34–36], $pp \rightarrow pn\rho^0\pi^+$ ($pp\rho^0\pi^0$) [37], $pp \rightarrow ppK^+K^-$ [38], $pp \rightarrow pp(\sigma\sigma, \rho^0\rho^0 \rightarrow \pi^+\pi^-\pi^+\pi^-)$ [39], $pp \rightarrow ppp\bar{p}$ [40], $pp \rightarrow pp(\phi\phi \rightarrow K^+K^-K^+K^-)$ [41], $pp \rightarrow pp(\phi \rightarrow K^+K^-, \mu^+\mu^-)$ [42], $pp \rightarrow ppf_1(1285)$ and $pp \rightarrow ppf_1(1420)$ [43]. The present paper aims to underline the importance of the study of the $pp \rightarrow pp(K^{*0}\bar{K}^{*0} \rightarrow K^+\pi^-K^-\pi^+)$ reaction.

Some effort to measure exclusive production of higher-multiplicity central systems at the energy $\sqrt{s} = 13$ TeV has been initiated by the ATLAS Collaboration; see, e.g., [44]. We think that a study of CEP of the $K^{*0}\bar{K}^{*0}$ pairs decaying into $K^+\pi^-K^-\pi^+$ should be quite rewarding for experimentalists. Our analysis are designed to facilitate the study of such processes at the LHC, for instance, by investigating in detail the continuum and tensor

resonance production.

The paper is organized as follows. In Sec. II we describe our theoretical framework. In Sec. III we show and discuss our numerical results. We determine the model parameters from a comparison to the WA102 experimental data for the reaction $pp \rightarrow pp K^{*0} \bar{K}^{*0}$. We also predict the total and differential cross sections for $pp \rightarrow pp(K^{*0} \bar{K}^{*0} \rightarrow K^+ K^- \pi^+ \pi^-)$ including typical kinematic cuts for the LHC experiments. The final section is devoted to the conclusions.

II. THEORETICAL FRAMEWORK

In the present paper we consider two processes shown in Fig. 1 that may contribute to the $K^+ \pi^- K^- \pi^+$ final state via an intermediate $K^{*0} \bar{K}^{*0} \equiv K^{*0}(892) \bar{K}^{*0}(892)$. Figure 1(a) shows the process with intermediate production of $f_2(1950)$ resonance,

$$pp \rightarrow pp (\mathbb{P}\mathbb{P} \rightarrow f_2(1950) \rightarrow K^{*0} \bar{K}^{*0}) \rightarrow pp K^+ \pi^- K^- \pi^+. \quad (2.1)$$

In Fig. 1(b) we have the continuum process

$$pp \rightarrow pp (\mathbb{P}\mathbb{P} \rightarrow K^{*0} \bar{K}^{*0}) \rightarrow pp K^+ \pi^- K^- \pi^+ \quad (2.2)$$

with the $K^{*0}(892)$ t/u -channel exchanges.

The processes (2.1) and (2.2) are expected to be most important ones at high energies since they involve pomeron exchange only. We can replace one or two pomerons by one or two $f_{2\mathbb{R}}$ reggeons. However, for the LHC collision energies and central $K^{*0} \bar{K}^{*0}$ production (midrapidity region) such $f_{2\mathbb{R}} f_{2\mathbb{R}}$ -, $f_{2\mathbb{R}} \mathbb{P}$ -, and $\mathbb{P} f_{2\mathbb{R}}$ -fusion contributions are expected to be small and we shall not consider them in our present paper.

We treat effectively the $2 \rightarrow 6$ processes (2.1) and (2.2) as arising from the $pp \rightarrow pp K^{*0} \bar{K}^{*0}$ reaction. The general cross-section formula can be written approximately as

$$\sigma_{2 \rightarrow 6} = \int_{m_K + m_\pi}^{\max\{m_{X_3}\}} \int_{m_K + m_\pi}^{\max\{m_{X_4}\}} \sigma_{2 \rightarrow 4}(\dots, m_{X_3}, m_{X_4}) f_{K^*}(m_{X_3}) f_{K^*}(m_{X_4}) dm_{X_3} dm_{X_4}. \quad (2.3)$$

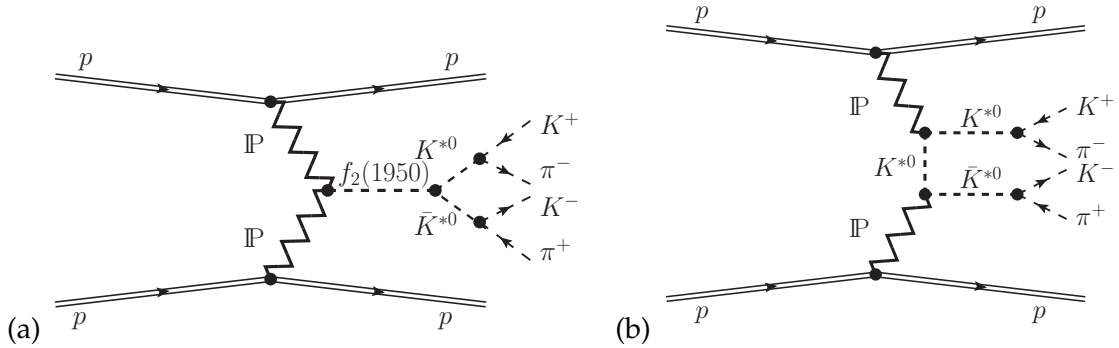


FIG. 1: The “Born level” diagrams for double pomeron central exclusive $K^{*0} \bar{K}^{*0}$ production and their subsequent decays into $K^+ \pi^- K^- \pi^+$ in proton-proton collisions: (a) $K^{*0} \bar{K}^{*0}$ production via the $f_2(1950)$ resonance; (b) continuum $K^{*0} \bar{K}^{*0}$ production.

We use for the calculation of decay processes $K^* \rightarrow K\pi$ the spectral function

$$f_{K^*}(m_{X_i}) = C_{K^*} \left(1 - \frac{(m_K + m_\pi)^2}{m_{X_i}^2} \right)^{3/2} \frac{\frac{2}{\pi} m_{X_i} m_{K^*} \Gamma_{K^*}}{(m_{X_i}^2 - m_{K^*}^2)^2 + m_{K^*}^2 \Gamma_{K^*}^2}, \quad (2.4)$$

where $i = 3, 4$, Γ_{K^*} is the total width of the $K^*(892)$ resonance and m_{K^*} its mass taken from [29], the factor C_{K^*} is found from the condition

$$\int_{m_K + m_\pi}^{\max\{m_X\}} f_{K^*}(m_X) dm_X = 1. \quad (2.5)$$

To include experimental cuts on outgoing pseudoscalar particles we perform the decays of $K^*(892)$ mesons isotropically in the K^* -meson rest frame and then use relativistic transformations to the overall center-of-mass frame.

Now we discuss the production of $K^{*0} \bar{K}^{*0}$ in proton-proton collisions,

$$p(p_a, \lambda_a) + p(p_b, \lambda_b) \rightarrow p(p_1, \lambda_1) + p(p_2, \lambda_2) + K^{*0}(p_3, \lambda_3) + \bar{K}^{*0}(p_4, \lambda_4), \quad (2.6)$$

where $p_{a,b}$, $p_{1,2}$ and $\lambda_{a,b}$, $\lambda_{1,2} = \pm \frac{1}{2}$ denote the four-momenta and helicities of the protons and $p_{3,4}$ and $\lambda_{3,4} = 0, \pm 1$ denote the four-momenta and helicities of the K^{*0} mesons, respectively.

The amplitude for the $2 \rightarrow 4$ reaction (2.6) can be written as

$$\mathcal{M}_{\lambda_a \lambda_b \rightarrow \lambda_1 \lambda_2 K^* \bar{K}^*} = \left(\epsilon_{\kappa_3}^{(K^*)}(\lambda_3) \right)^* \left(\epsilon_{\kappa_4}^{(\bar{K}^*)}(\lambda_4) \right)^* \mathcal{M}_{\lambda_a \lambda_b \rightarrow \lambda_1 \lambda_2 K^* \bar{K}^*}^{\kappa_3 \kappa_4}, \quad (2.7)$$

where $\epsilon_{\kappa}^{(K^*)}$ are the polarisation vectors of the K^* mesons. Taking into account summation over the K^* polarisations we get for the amplitudes squared [to be inserted in $\sigma_{2 \rightarrow 4}$ in Eq. (2.3)]

$$\frac{1}{4} \sum_{\text{spins}} \left| \mathcal{M}_{\lambda_a \lambda_b \rightarrow \lambda_1 \lambda_2 K^* \bar{K}^*} \right|^2 = \frac{1}{4} \sum_{\lambda_a, \lambda_b, \lambda_1, \lambda_2} \left(\mathcal{M}_{\lambda_a \lambda_b \rightarrow \lambda_1 \lambda_2 K^* \bar{K}^*}^{\sigma_3 \sigma_4} \right)^* \mathcal{M}_{\lambda_a \lambda_b \rightarrow \lambda_1 \lambda_2 K^* \bar{K}^*}^{\rho_3 \rho_4} g_{\sigma_3 \rho_3} g_{\sigma_4 \rho_4}. \quad (2.8)$$

We take into account two main processes shown by the diagrams in Fig. 1. The full amplitude is then the sum of the $f_2(1950)$ resonance term and the K^{*0} -exchange continuum term:

$$\mathcal{M}_{\lambda_a \lambda_b \rightarrow \lambda_1 \lambda_2 K^* \bar{K}^*}^{\kappa_3 \kappa_4} = \mathcal{M}_{\lambda_a \lambda_b \rightarrow \lambda_1 \lambda_2 K^* \bar{K}^*}^{(\mathbb{P}\mathbb{P} \rightarrow f_2 \rightarrow K^* \bar{K}^*) \kappa_3 \kappa_4} + \mathcal{M}_{\lambda_a \lambda_b \rightarrow \lambda_1 \lambda_2 K^* \bar{K}^*}^{(K^* \text{-exchange}) \kappa_3 \kappa_4}. \quad (2.9)$$

In our exploratory study we consider these terms separately, i.e., we neglect interference effects between the resonant $f_2(1950) \rightarrow K^{*0} \bar{K}^{*0}$ and the continuum $K^{*0} \bar{K}^{*0}$ processes.

To give the full physical amplitude for the reaction (2.6) we include absorptive corrections to the Born amplitudes in the one-channel eikonal approximation; see, e.g., Sec. 3.3 of [34]. In practice we work with the amplitudes in the high-energy approximation, i.e., assume s -channel helicity conservation for the protons.

A. $f_2(1950)$ resonance contribution

Now we consider the amplitude representing by the diagram in Fig. 1(a) but limiting to the final state $ppK^{*0}\bar{K}^{*0}$.

The Born-level amplitude for the $\mathbb{P}\mathbb{P}$ -fusion process through the s -channel $f_2(1950)$ -meson exchange is given by

$$\begin{aligned} \mathcal{M}_{\lambda_a \lambda_b \rightarrow \lambda_1 \lambda_2 K^* \bar{K}^*}^{(\mathbb{P}\mathbb{P} \rightarrow f_2 \rightarrow K^* \bar{K}^*) \kappa_3 \kappa_4} = & (-i) \bar{u}(p_1, \lambda_1) i\Gamma^{(\mathbb{P}pp) \mu_1 \nu_1}(p_1, p_a) u(p_a, \lambda_a) i\Delta_{\mu_1 \nu_1, \alpha_1 \beta_1}^{(\mathbb{P})}(s_1, t_1) \\ & \times i\Gamma^{(\mathbb{P}\mathbb{P}f_2) \alpha_1 \beta_1, \alpha_2 \beta_2, \rho \sigma}(q_1, q_2) i\Delta_{\rho \sigma, \alpha \beta}^{(f_2)}(p_{34}) i\Gamma^{(f_2 K^* \bar{K}^*) \alpha \beta \kappa_3 \kappa_4}(p_3, p_4) \\ & \times i\Delta_{\alpha_2 \beta_2, \mu_2 \nu_2}^{(\mathbb{P})}(s_2, t_2) \bar{u}(p_2, \lambda_2) i\Gamma^{(\mathbb{P}pp) \mu_2 \nu_2}(p_2, p_b) u(p_b, \lambda_b), \end{aligned} \quad (2.10)$$

where $s_1 = (p_1 + p_3 + p_4)^2$, $s_2 = (p_2 + p_3 + p_4)^2$, $q_1 = p_a - p_1$, $q_2 = p_b - p_2$, $t_1 = q_1^2$, $t_2 = q_2^2$, and $p_{34} = q_1 + q_2 = p_3 + p_4$. Here $\Gamma^{(\mathbb{P}pp)}$ and $\Delta^{(\mathbb{P})}$ denote the effective proton vertex function and propagator, respectively, for the tensor-pomeron exchange. The corresponding expressions, as given in Sec. 3 of [26], are as follows

$$i\Gamma_{\mu\nu}^{(\mathbb{P}pp)}(p', p) = -i3\beta_{\mathbb{P}NN}F_1(t) \left\{ \frac{1}{2} [\gamma_\mu(p' + p)_\nu + \gamma_\nu(p' + p)_\mu] - \frac{1}{4}g_{\mu\nu}(\not{p}' + \not{p}) \right\}, \quad (2.11)$$

$$i\Delta_{\mu\nu, \kappa\lambda}^{(\mathbb{P})}(s, t) = \frac{1}{4s} \left(g_{\mu\kappa}g_{\nu\lambda} + g_{\mu\lambda}g_{\nu\kappa} - \frac{1}{2}g_{\mu\nu}g_{\kappa\lambda} \right) (-is\alpha'_{\mathbb{P}})^{\alpha_{\mathbb{P}}(t)-1}, \quad (2.12)$$

where $\beta_{\mathbb{P}NN} = 1.87 \text{ GeV}^{-1}$ and $F_1(t)$ is the Dirac form factor of the proton. For extensive discussions of the properties of these terms we refer to [26]. In (2.12) the pomeron trajectory $\alpha_{\mathbb{P}}(t)$ is assumed to be of standard linear form, see e.g. [45, 46],

$$\begin{aligned} \alpha_{\mathbb{P}}(t) &= \alpha_{\mathbb{P}}(0) + \alpha'_{\mathbb{P}} t, \\ \alpha_{\mathbb{P}}(0) &= 1.0808, \quad \alpha'_{\mathbb{P}} = 0.25 \text{ GeV}^{-2}. \end{aligned} \quad (2.13)$$

The $\mathbb{P}\mathbb{P}f_2$ vertex, including a form factor, can be written as

$$i\Gamma_{\mu\nu, \kappa\lambda, \rho\sigma}^{(\mathbb{P}\mathbb{P}f_2)}(q_1, q_2) = \left(i\Gamma_{\mu\nu, \kappa\lambda, \rho\sigma}^{(\mathbb{P}\mathbb{P}f_2)(1)}|_{\text{bare}} + \sum_{j=2}^7 i\Gamma_{\mu\nu, \kappa\lambda, \rho\sigma}^{(\mathbb{P}\mathbb{P}f_2)(j)}(q_1, q_2)|_{\text{bare}} \right) \tilde{F}^{(\mathbb{P}\mathbb{P}f_2)}(q_1^2, q_2^2, p_{34}^2). \quad (2.14)$$

A possible choice for the $i\Gamma_{\mu\nu, \kappa\lambda, \rho\sigma}^{(\mathbb{P}\mathbb{P}f_2)(j)}$ coupling terms $j = 1, \dots, 7$ is given in Appendix A of [35]. The couplings $j = 1, \dots, 7$ can be associate to the following orbital angular momentum and spin of the two “real pomerons” (l, S) values: $(0, 2)$, $(2, 0) - (2, 2)$, $(2, 0) + (2, 2)$, $(2, 4)$, $(4, 2)$, $(4, 4)$, $(6, 4)$, respectively. In the following we shall, for the purpose of orientation, assume that only the $j = 1$ coupling in (2.14), corresponding to the lowest values of (l, S) , that is $(l, S) = (0, 2)$, is unequal to zero. The expressions for $j = 1$ vertex is as

follows:¹

$$i\Gamma_{\mu\nu,\kappa\lambda,\rho\sigma}^{(\mathbb{P}\mathbb{P}f_2)(1)}|_{\text{bare}} = 2i g_{\mathbb{P}\mathbb{P}f_2}^{(1)} M_0 R_{\mu\nu\mu_1\nu_1} R_{\kappa\lambda\alpha_1\lambda_1} R_{\rho\sigma\rho_1\sigma_1} g^{\nu_1\alpha_1} g^{\lambda_1\rho_1} g^{\sigma_1\mu_1}, \quad (2.15)$$

$$R_{\mu\nu\kappa\lambda} = \frac{1}{2}g_{\mu\kappa}g_{\nu\lambda} + \frac{1}{2}g_{\mu\lambda}g_{\nu\kappa} - \frac{1}{4}g_{\mu\nu}g_{\kappa\lambda}, \quad (2.16)$$

see (A12) of [35]. In (2.15), $M_0 \equiv 1 \text{ GeV}$ and the $g_{\mathbb{P}\mathbb{P}f_2}^{(1)}$ is dimensionless coupling constant which should be fitted to experimental data. We take the factorized form for the $\mathbb{P}\mathbb{P}f_2$ form factor in (2.14):

$$\tilde{F}^{(\mathbb{P}\mathbb{P}f_2)}(q_1^2, q_2^2, p_{34}^2) = \tilde{F}_M(q_1^2) \tilde{F}_M(q_2^2) F^{(\mathbb{P}\mathbb{P}f_2)}(p_{34}^2); \quad (2.17)$$

$$\tilde{F}_M(t) = \frac{1}{1 - t/\tilde{\Lambda}_0^2}. \quad (2.18)$$

The form factor $F^{(\mathbb{P}\mathbb{P}f_2)}$ is normalized to unity at the on-shell point $F^{(\mathbb{P}\mathbb{P}f_2)}(m_{f_2}^2) = 1$ and parametrised in two ways:

$$F^{(\mathbb{P}\mathbb{P}f_2)}(p_{34}^2) = \exp\left(\frac{-(p_{34}^2 - m_{f_2}^2)^2}{\Lambda_{f_2,E}^4}\right), \quad (2.19)$$

$$F^{(\mathbb{P}\mathbb{P}f_2)}(p_{34}^2) = \frac{\Lambda_{f_2,P}^4}{\Lambda_{f_2,P}^4 + (p_{34}^2 - m_{f_2}^2)^2}. \quad (2.20)$$

The cutoff parameters $\tilde{\Lambda}_0$, $\Lambda_{f_2,E}$ and $\Lambda_{f_2,P}$ in (2.18), (2.19) and (2.20), respectively, are treated as free parameters which could be adjusted to fit the experimental data.

We use in (2.10) the tensor-meson propagator with the simple Breit-Wigner form; see (3.35) of [41]. A better representation for the propagator could be constructed using the methods of [26, 47], used there for the ρ^0 and $f_2(1270)$ propagators. In our calculations we take the nominal values for the $f_2(1950)$ from [29]:

$$\begin{aligned} m_{f_2} &= (1936 \pm 12) \text{ MeV}, \\ \Gamma_{f_2} &= (464 \pm 24) \text{ MeV}. \end{aligned} \quad (2.21)$$

For the $f_2 K^* \bar{K}^*$ vertex function we take the same ansatz as for the $f_2 \phi \phi$ vertex defined in (3.32) of [41]. The $f_2 K^* \bar{K}^*$ vertex is as follows:

$$\begin{aligned} i\Gamma_{\mu\nu\kappa\lambda}^{(f_2 K^* \bar{K}^*)}(p_3, p_4) &= i \frac{2}{M_0^3} g'_{f_2 K^* \bar{K}^*} \Gamma_{\mu\nu\kappa\lambda}^{(0)}(p_3, p_4) F'^{(f_2 K^* \bar{K}^*)}(p_{34}^2) \\ &\quad - i \frac{1}{M_0^3} g''_{f_2 K^* \bar{K}^*} \Gamma_{\mu\nu\kappa\lambda}^{(2)}(p_3, p_4) F''^{(f_2 K^* \bar{K}^*)}(p_{34}^2) \end{aligned} \quad (2.22)$$

¹ Here the label “bare” is used for a vertex, as derived from a corresponding coupling Lagrangian in Appendix A of [35] without a form-factor function.

with two rank-four tensor functions,

$$\begin{aligned}\Gamma_{\mu\nu\kappa\lambda}^{(0)}(p_3, p_4) &= \left[(p_3 \cdot p_4) g_{\mu\nu} - p_{4\mu} p_{3\nu} \right] \left[p_{3\kappa} p_{4\lambda} + p_{4\kappa} p_{3\lambda} - \frac{1}{2} (p_3 \cdot p_4) g_{\kappa\lambda} \right], \quad (2.23) \\ \Gamma_{\mu\nu\kappa\lambda}^{(2)}(p_3, p_4) &= (p_3 \cdot p_4) (g_{\mu\kappa} g_{\nu\lambda} + g_{\mu\lambda} g_{\nu\kappa}) + g_{\mu\nu} (p_{3\kappa} p_{4\lambda} + p_{4\kappa} p_{3\lambda}) \\ &\quad - p_{3\nu} p_{4\lambda} g_{\mu\kappa} - p_{3\nu} p_{4\kappa} g_{\mu\lambda} - p_{4\mu} p_{3\lambda} g_{\nu\kappa} - p_{4\mu} p_{3\kappa} g_{\nu\lambda} \\ &\quad - [(p_3 \cdot p_4) g_{\mu\nu} - p_{4\mu} p_{3\nu}] g_{\kappa\lambda}; \quad (2.24)\end{aligned}$$

see Eqs. (3.18) and (3.19) of [26]. The coupling parameters $g'_{f_2 K^* \bar{K}^*}$ and $g''_{f_2 K^* \bar{K}^*}$ are dimensionless. Different form factors F' and F'' are allowed *a priori*. We assume, in the present exploratory study, that

$$F'(f_2 K^* \bar{K}^*)(p_{34}^2) = F''(f_2 K^* \bar{K}^*)(p_{34}^2) = F(\mathbb{P} f_2)(p_{34}^2) \quad (2.25)$$

and for the cutoff parameters to be the same, $\Lambda'_{f_2} = \Lambda''_{f_2} = \Lambda_{f_2, E}$ or $\Lambda_{f_2, P}$; see (2.19) and (2.20).

One has to keep in mind that relative signs of couplings have physical significance, for instance, the relative sign of g' and g'' . However, for orientation purposes, in the calculation we treat them separately and do not fix the sign of the f_2 couplings. With our choice to keep only one $\mathbb{P} f_2(1950)$ coupling from (2.14), namely (2.15) with $g_{\mathbb{P} f_2}^{(1)}$, the results will depend on the product of the couplings $g_{\mathbb{P} f_2}^{(1)} g'_{f_2 K^* \bar{K}^*}$ and $g_{\mathbb{P} f_2}^{(1)} g''_{f_2 K^* \bar{K}^*}$ with $g'_{f_2 K^* \bar{K}^*}$ and $g''_{f_2 K^* \bar{K}^*}$ given in (2.22). In the following we assume that only either the first or the second of the above products of couplings is nonzero.

B. Diffractive continuum contribution

The diagram for the continuum $K^{*0} \bar{K}^{*0}$ with an intermediate K^{*0} exchange is shown in Fig. 1 (b). The Born-level amplitude can be written as the sum

$$\mathcal{M}_{\lambda_a \lambda_b \rightarrow \lambda_1 \lambda_2 K^* \bar{K}^*}^{(K^* \text{-exchange}) \kappa_3 \kappa_4} = \mathcal{M}_{\lambda_a \lambda_b \rightarrow \lambda_1 \lambda_2 K^* \bar{K}^*}^{(\hat{t}) \kappa_3 \kappa_4} + \mathcal{M}_{\lambda_a \lambda_b \rightarrow \lambda_1 \lambda_2 K^* \bar{K}^*}^{(\hat{u}) \kappa_3 \kappa_4} \quad (2.26)$$

with the \hat{t} - and \hat{u} -channel amplitudes:

$$\begin{aligned}\mathcal{M}_{\kappa_3 \kappa_4}^{(\hat{t})} &= (-i) \bar{u}(p_1, \lambda_1) i\Gamma_{\mu_1 \nu_1}^{(\mathbb{P} p p)}(p_1, p_a) u(p_a, \lambda_a) i\Delta^{(\mathbb{P}) \mu_1 \nu_1, \alpha_1 \beta_1}(s_{13}, t_1) \\ &\quad \times i\Gamma_{\kappa_1 \kappa_3 \alpha_1 \beta_1}^{(\mathbb{P} K^* K^*)}(\hat{p}_t, -p_3) i\Delta^{(K^*) \kappa_1 \kappa_2}(\hat{p}_t) i\Gamma_{\kappa_4 \kappa_2 \alpha_2 \beta_2}^{(\mathbb{P} K^* K^*)}(p_4, \hat{p}_t) \\ &\quad \times i\Delta^{(\mathbb{P}) \alpha_2 \beta_2, \mu_2 \nu_2}(s_{24}, t_2) \bar{u}(p_2, \lambda_2) i\Gamma_{\mu_2 \nu_2}^{(\mathbb{P} p p)}(p_2, p_b) u(p_b, \lambda_b), \quad (2.27)\end{aligned}$$

$$\begin{aligned}\mathcal{M}_{\kappa_3 \kappa_4}^{(\hat{u})} &= (-i) \bar{u}(p_1, \lambda_1) i\Gamma_{\mu_1 \nu_1}^{(\mathbb{P} p p)}(p_1, p_a) u(p_a, \lambda_a) i\Delta^{(\mathbb{P}) \mu_1 \nu_1, \alpha_1 \beta_1}(s_{14}, t_1) \\ &\quad \times i\Gamma_{\kappa_4 \kappa_1 \alpha_1 \beta_1}^{(\mathbb{P} K^* K^*)}(p_4, \hat{p}_u) i\Delta^{(K^*) \kappa_1 \kappa_2}(\hat{p}_u) i\Gamma_{\kappa_2 \kappa_3 \alpha_2 \beta_2}^{(\mathbb{P} K^* K^*)}(\hat{p}_u, -p_3) \\ &\quad \times i\Delta^{(\mathbb{P}) \alpha_2 \beta_2, \mu_2 \nu_2}(s_{23}, t_2) \bar{u}(p_2, \lambda_2) i\Gamma_{\mu_2 \nu_2}^{(\mathbb{P} p p)}(p_2, p_b) u(p_b, \lambda_b), \quad (2.28)\end{aligned}$$

where $\hat{p}_t = p_a - p_1 - p_3$, $\hat{p}_u = p_4 - p_a + p_1$, $s_{ij} = (p_i + p_j)^2$.

Our ansatz for the $\mathbb{P}K^*K^*$ vertex follows the one for the $\mathbb{P}\rho\rho$ in (3.47) of [26] with the replacements $a_{\mathbb{P}\rho\rho} \rightarrow a_{\mathbb{P}K^*K^*}$ and $b_{\mathbb{P}\rho\rho} \rightarrow b_{\mathbb{P}K^*K^*}$; see also Eqs. (3.12)–(3.14) of [41]. With k', μ and k, ν the momentum and vector index of the outgoing and incoming K^* , respectively, and $\kappa\lambda$ the tensor-pomeron indices, the $\mathbb{P}K^*K^*$ vertex reads

$$i\Gamma_{\mu\nu\kappa\lambda}^{(\mathbb{P}K^*K^*)}(k', k) = iF_M((k' - k)^2) \left[2a_{\mathbb{P}K^*K^*} \Gamma_{\mu\nu\kappa\lambda}^{(0)}(k', -k) - b_{\mathbb{P}K^*K^*} \Gamma_{\mu\nu\kappa\lambda}^{(2)}(k', -k) \right]. \quad (2.29)$$

Here the coupling parameters a and b have dimensions GeV^{-3} and GeV^{-1} , respectively. We take for $F_M(t)$ the form given in (2.18) but with $\tilde{\Lambda}_0^2 \rightarrow \Lambda_0^2$,

$$F_M(t) = \frac{1}{1 - t/\Lambda_0^2}. \quad (2.30)$$

The amplitudes (2.27) and (2.28) also contain a form factors for the off-shell dependencies of the intermediate K^* mesons, $\hat{F}_{K^*}(\hat{p}_t^2)$ and $\hat{F}_{K^*}(\hat{p}_u^2)$, respectively. These form factors are parametrised in the exponential form

$$\hat{F}_{K^*}(\hat{p}^2) = \exp\left(\frac{\hat{p}^2 - m_{K^*}^2}{\Lambda_{\text{off,E}}^2}\right). \quad (2.31)$$

We assume that only one coupling in (2.29) contributes, that is, $a_{\mathbb{P}K^*K^*} \neq 0$ or $b_{\mathbb{P}K^*K^*} \neq 0$. With this assumption, the sign of a or b does not matter as the corresponding coupling occurs twice in the amplitude. The $\mathbb{P}K^*K^*$ coupling parameters (a , b) and the cutoff parameters (Λ_0 , $\Lambda_{\text{off,E}}$) could be adjusted to experimental data.

For the K^* -meson propagator $\Delta_{\kappa_1\kappa_2}^{(K^*)}$ using the properties of tensorial functions we can make the replacement $\Delta_{\kappa_1\kappa_2}^{(K^*)}(\hat{p}^2) \rightarrow -g_{\kappa_1\kappa_2} \Delta_T^{(K^*)}(\hat{p}^2)$. We take for $\hat{p}^2 < 0$ the simple expression $(\Delta_T^{(K^*)}(\hat{p}^2))^{-1} = \hat{p}^2 - m_{K^*}^2$.

We should take into account the reggeization of intermediate K^* meson. In [48] it was argued that the reggeization should not be applied when the rapidity distance between two centrally produced mesons, $Y_{\text{diff}} = Y_3 - Y_4$, tends to zero (i.e. for $|\hat{p}^2| \sim s_{34}$). We follow (3.25) of [41] and use a formula for the K^* propagator which interpolates continuously between the regions of low Y_{diff} , where we use the standard K^* propagator, and of high Y_{diff} where we use the reggeized form:

$$\begin{aligned} \Delta_{\kappa_1\kappa_2}^{(K^*)}(\hat{p}) &\rightarrow \Delta_{\kappa_1\kappa_2}^{(K^*)}(\hat{p}) F(Y_{\text{diff}}) + \Delta_{\kappa_1\kappa_2}^{(K^*)}(\hat{p}) [1 - F(Y_{\text{diff}})] \left(\exp(i\phi(s_{34})) \frac{s_{34}}{s_{\text{thr}}} \right)^{\alpha_{K^*}(\hat{p}^2)-1}, \\ F(Y_{\text{diff}}) &= \exp(-c_y |Y_{\text{diff}}|), \\ \phi(s_{34}) &= \frac{\pi}{2} \exp\left(\frac{s_{\text{thr}} - s_{34}}{s_{\text{thr}}}\right) - \frac{\pi}{2}, \end{aligned} \quad (2.32)$$

where $s_{34} = M_{K^*0\bar{K}^*0}^2$, $s_{\text{thr}} = 4m_{K^*0}^2$, and c_y is an unknown parameter which measures how fast one approaches to the Regge regime. Here we take $c_y = 2$. This choice is motivated by Fig. 6 of [41].

We assume for the K^* Regge trajectory a simple linear form [see (5.3.1) of [49]]

$$\alpha_{K^*}(\hat{p}^2) = \alpha_{K^*}(0) + \alpha'_{K^*} \hat{p}^2, \quad (2.33)$$

with the intercept and slope of the trajectory $\alpha_{K^*}(0) = 0.3$ and $\alpha'_{K^*} = 0.9 \text{ GeV}^{-2}$, respectively. We will also show the results using a nonlinear Regge trajectory² for the K^* mesons, the so-called “square-root” trajectory, parametrised as [50]

$$\alpha_{K^*}(\hat{p}^2) = \alpha_{K^*}(0) + \gamma \left(\sqrt{T_{K^*}} - \sqrt{T_{K^*} - \hat{p}^2} \right), \quad (2.34)$$

where γ governs the slope of the trajectory and T_{K^*} denotes the trajectory termination point. The parameters are fixed to be $\alpha_{K^*}(0) = 0.414$, $\gamma = 3.65 \text{ GeV}^{-1}$, $\sqrt{T_{K^*}} = 2.58 \text{ GeV}$.

III. NUMERICAL RESULTS AND DISCUSSIONS

In this section we wish to present first results for the $pp \rightarrow ppK^{*0}(892)\bar{K}^{*0}(892)$ reaction and for the $pp \rightarrow ppK^+\pi^-K^-\pi^+$ reaction corresponding to the diagrams in Fig. 1.

A. Comparison with the WA102 data

It was noticed by the WA102 Collaboration [10] that the cross section for the production of a $K^*(892)\bar{K}^*(892)$ system slowly rises with rising the center-of-mass energy \sqrt{s} . The experimental results, for the same interval on the central $K^*\bar{K}^*$ system $|x_F| \leq 0.2$, are $\sigma_{\text{exp}} = 67 \pm 16 \text{ nb}$ at $\sqrt{s} = 12.7 \text{ GeV}$ [8], $\sigma_{\text{exp}} = 70 \pm 14 \text{ nb}$ at $\sqrt{s} = 23.8 \text{ GeV}$ [9], and $\sigma_{\text{exp}} = 85 \pm 10 \text{ nb}$ at $\sqrt{s} = 29.1 \text{ GeV}$ [10]. This suggests that the pomeron-pomeron fusion mechanism is the dominant one for the $pp \rightarrow ppK^{*0}\bar{K}^{*0}$ reaction in the above energy range. A similar behaviour of the cross section as a function \sqrt{s} was observed experimentally also for the $\phi\phi$ production [11]. In the following we neglect, therefore, secondary reggeon exchanges.

In Fig. 2 we show the invariant mass distributions for the $\mathbb{P}\mathbb{P} \rightarrow f_2(1950)$ mechanism together with the WA102 experimental data from Fig. 2 of [10]. The data points have been normalised to the mean value of the total cross section $\sigma_{\text{exp}} = 85 \pm 10 \text{ nb}$ from [10]. For the purpose of orientation, we have assumed, that in the $\mathbb{P}\mathbb{P}f_2(1950)$ vertex (2.14) only $g^{(1)}$ coupling constant is unequal to zero. We have checked that for the distributions studied here the choice of $\mathbb{P}\mathbb{P}f_2$ coupling is not important. This is similar to what was found in [41] for the reaction $pp \rightarrow pp(\mathbb{P}\mathbb{P} \rightarrow f_2(2340) \rightarrow \phi\phi)$. In the calculation we take only one $\mathbb{P}\mathbb{P}f_2$ coupling [$g_{\mathbb{P}\mathbb{P}f_2}^{(1)}$ from (2.14)] and only one $f_2K^*\bar{K}^*$ coupling [$g'_{f_2K^*\bar{K}^*}$ or $g''_{f_2K^*\bar{K}^*}$ from (2.22)]. The results shown in the left panel correspond to the product of the couplings $|g^{(1)} \times g'| = 28.0$, while the results in the right panel are for $|g^{(1)} \times g''| = 11.0$. We note that only the absolute value of both products for fixed the cutoff parameter of the f_2 -meson off-shell form factor (2.25) can be determined. We have checked that in both cases the results for the product of the form factors $F^{(\mathbb{P}\mathbb{P}f_2)}(p_{34}^2) \times F^{(f_2K^*\bar{K}^*)}(p_{34}^2)$ assuming the same type of form factors, (2.19) or (2.20), are similar. In the following we choose in the calculation only the power form (2.20) with the cutoff parameter $\Lambda_{f_2,P}$ (2.22). It is clearly seen from the left panel that the result without these form factors, i.e., for $p_{34}^2 = m_{f_2}^2$,

² For the discussion of nonlinear Regge trajectories see Ref. [20] and references therein.

is well above the WA102 experimental data for $M_{K^*0\bar{K}^*0} > 2.1$ GeV. The results are very sensitive to the choice of the cutoff parameters. It can be observed that as $\Lambda_{f_2,P}$ decreases then mainly the right flank of the resonance is reduced and thus it becomes narrower. For $\Lambda_{f_2,P} = 1.6 - 2.0$ GeV and $|g^{(1)} \times g''| = 11.0$ (see the short-dashed lines in the right panel) an agreement with the WA102 data in the invariant mass range $M_{K^*0\bar{K}^*0} \in (1.9, 2.2)$ GeV can be obtained.

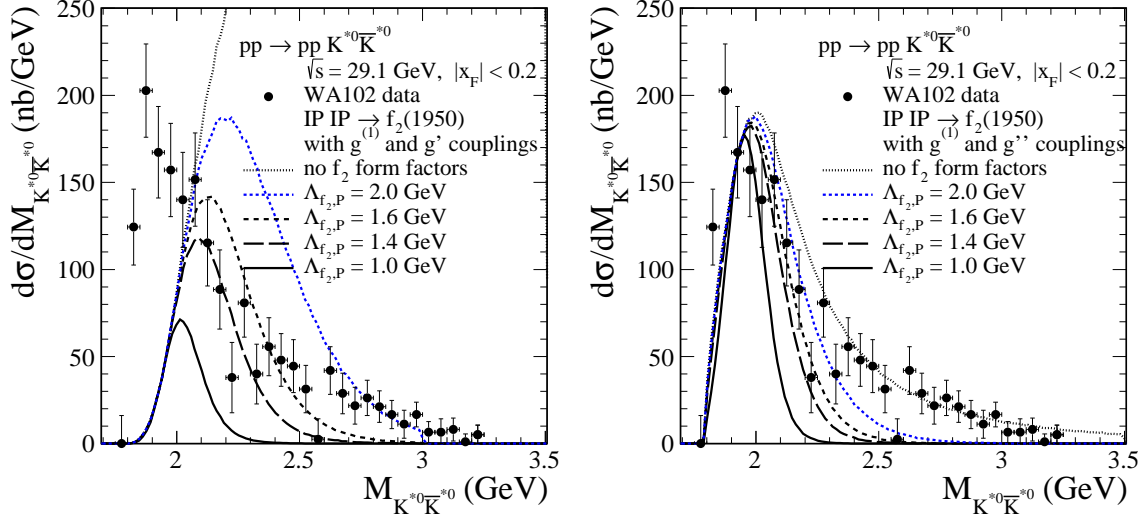


FIG. 2: The distributions in $K^*0\bar{K}^*0$ invariant mass compared to the WA102 data [10] for the $\text{IP} \text{IP} \rightarrow f_2(1950)$ contribution. The calculations were done for $\sqrt{s} = 29.1$ GeV and for $|x_F| \leq 0.2$ of the central $K^*\bar{K}^*$ system. The data points have been normalized to the total cross section $\sigma_{\text{exp}} = 85$ nb. We show results for the two sets of coupling constants $|g_{\text{PP}f_2}^{(1)} g'_{f_2K^*\bar{K}^*}| = 28.0$ (left panel) and $|g_{\text{PP}f_2}^{(1)} g''_{f_2K^*\bar{K}^*}| = 11.0$ (right panel) and for various cutoff parameters $\Lambda_{f_2,P} = 1.0, 1.4, 1.6$, and 2.0 GeV in the form factors (2.20) and (2.25) describing the off-shellness of the f_2 meson. We have taken here $\tilde{\Lambda}_0^2 = 0.5 \text{ GeV}^2$ (2.18). In addition, we show also a naive results that corresponds to the calculations without these form factors. The absorption effects are included.

In Figs. 3 and 4 we show different differential observables in Y_{diff} , the rapidity difference between the two K^*0 mesons, in $|t|$, the transferred four-momentum squared from one of the proton vertices ($t = t_1$ or t_2), and in ϕ_{pp} , the azimuthal angle between the transverse momentum vectors $\mathbf{p}_{t,1}$ and $\mathbf{p}_{t,2}$ of the outgoing protons. We present the results obtained separately for different couplings taking into account the absorptive corrections. In the left panel of Fig. 4 we show results for the individual j coupling terms $g_{\text{PP}f_2}^{(j)} \times g'_{f_2K^*\bar{K}^*}$ (only for five terms), while in the right panel for $g_{\text{PP}f_2}^{(j)} \times g''_{f_2K^*\bar{K}^*}$. For illustration, the results have been obtained with coupling constants $|g^{(j)} \times g'| = 1.0$ (left panel) and $|g^{(j)} \times g''| = 1.0$ (right panel). The shape of the Y_{diff} distribution depends on the choice of the $f_2(1950)K^*\bar{K}^*$ coupling. It can be expected that this variable will be very helpful in determining the $f_2K^*\bar{K}^*$ coupling using data from LHC measurements, in particular, if they cover a wider range of rapidities; see the discussion in Sec. IV B of Ref. [41]. The shapes of the distributions in Y_{diff} within each group are similar except of $j = 2$ term. In Fig. 4 we show the results only for the second group with the g'' coupling. We have

checked that with the g' coupling the shapes of the distributions for these observables are very similar. Compared to the WA102 data from [10] that will be presented later (Fig. 6), it can be concluded that the terms $j = 2$ and 5 can be excluded. We find that the three cases, $j = 1, 3$ and 4, give similar characteristics for the WA102 data. In the following considerations, for simplicity, we assume only one set of couplings, namely, $j = 1$ $g_{\mathbb{P}\mathbb{P}f_2}^{(1)}$ and $g_{f_2K^*\bar{K}^*}''$.

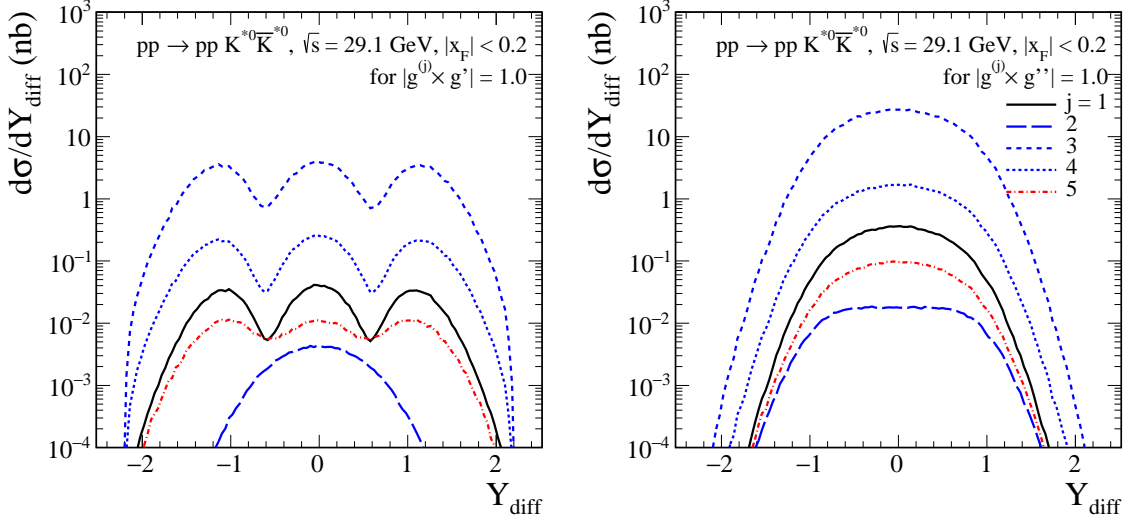


FIG. 3: The distributions in Y_{diff} for the process $\mathbb{P}\mathbb{P} \rightarrow f_2(1950) \rightarrow K^{*0}\bar{K}^{*0}$. The calculations were done for $\sqrt{s} = 29.1$ GeV and for $|x_F| \leq 0.2$ of the central $K^*\bar{K}^*$ system. We show the individual contributions of the different $\mathbb{P}\mathbb{P}f_2$ couplings (2.14) with index j . We have taken here $\tilde{\Lambda}_0^2 = 0.5$ GeV² and $\Lambda_{f_2,P} = 1.6$ GeV. The results in the left panel have been obtained with coupling constants $|g_{\mathbb{P}\mathbb{P}f_2}^{(j)} g'_{f_2K^*\bar{K}^*}| = 1.0$, while the results in the right panel with $|g_{\mathbb{P}\mathbb{P}f_2}^{(j)} g''_{f_2K^*\bar{K}^*}| = 1.0$. The absorption effects are included.

Now we turn to the diffractive continuum mechanism. In Fig. 5 we show the results for the continuum process via the K^{*0} -meson exchange including the reggeization effect given in (2.32), (2.33). In our calculation we take $\Lambda_{\text{off},E} = 1.6$ GeV in (2.31). We compare our results assuming only one type of the $\mathbb{P}K^*K^*$ coupling, a or b , to the WA102 experimental data for the $M_{K^{*0}\bar{K}^{*0}}$ distribution. Our model calculation with only the b -type coupling ($a = 0$ and $|b| = 4.37$ GeV⁻¹) describes the experimental data reasonably well, although, because of large experimental error bars, a small contribution from the a -type coupling cannot be ruled out. The option $|a| = 1.83$ GeV⁻³ and $b = 0$ (see the dashed line) is clearly ruled out by the WA102 data. We cannot also completely rule out some contribution of the $f_2(1950)$ resonance. We wish to point out that the interference effects possible between these terms may also play an important role; see [41]. This requires further analysis and will only be meaningful once experiments with better statistics become available. Hopefully this will be the case at the LHC.

In Fig. 6 we show the results for the $|t|$ and ϕ_{pp} distributions together with the experimental data from Fig. 3 of [10]. The data points have been normalised to the mean value of the total cross section ($\sigma_{\text{exp}} = 85 \pm 10$ nb) from [10]. We present results only for the continuum K^{*0} -exchange contribution without (the top lines) and with (the bottom lines)

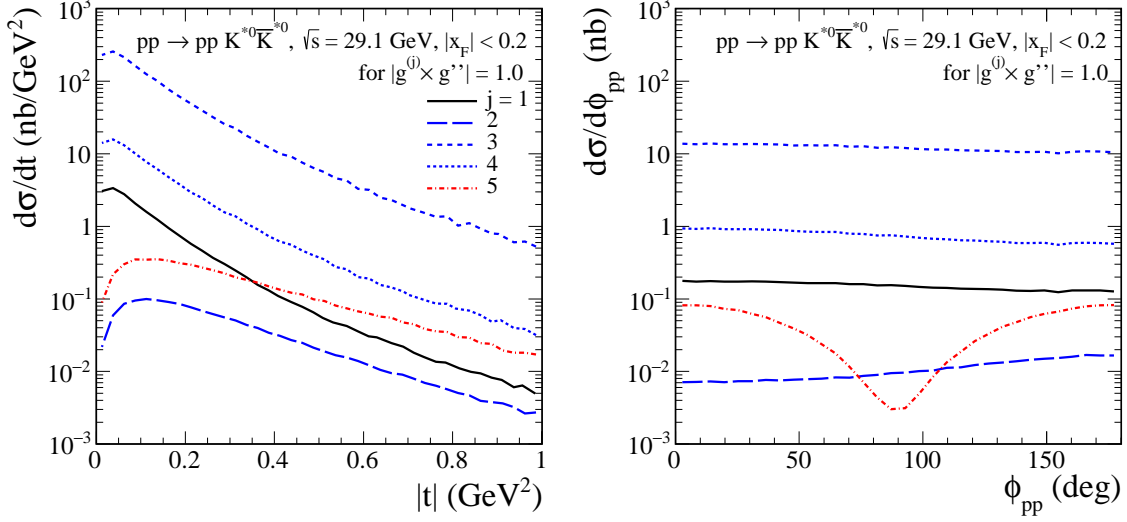


FIG. 4: . The $|t|$ (left panel) and ϕ_{pp} (right panel) distributions for the $pp \rightarrow pp(\mathbb{P}\mathbb{P} \rightarrow f_2(1950) \rightarrow K^{*0} \bar{K}^{*0})$ reaction for the WA102 kinematics. The meaning of the lines is the same as in the right panel of Fig. 3. The calculation was done for $|g_{\mathbb{P}\mathbb{P}f_2}^{(j)} g''_{f_2 K^* \bar{K}^*}| = 1.0$. The absorption effects are included.

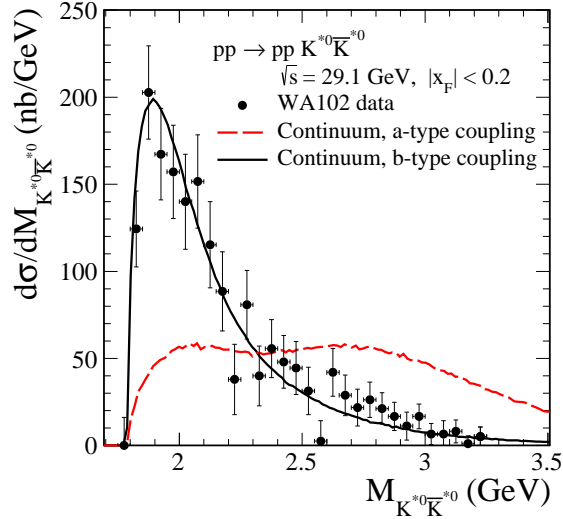


FIG. 5: The same as in Fig. 2 but here we show the theoretical results for the continuum mechanism. We show results for the two type of the $\mathbb{P}K^*K^*$ coupling considered separately, $a_{\mathbb{P}K^*K^*}$ and $b_{\mathbb{P}K^*K^*}$, occurring in (2.29). The results are normalized to the same value $\sigma = 85$ nb. The red dashed line corresponds to $|a| = 1.83$ GeV^{-3} and $b = 0$, while the black solid line corresponds to $a = 0$ and $|b| = 4.37$ GeV^{-1} . The absorption effects are included.

the absorption effects included in the calculations. We have checked that the $f_2(1950)$ -exchange contribution (with $g^{(1)}$ and g' or g'' couplings) has a very similar shape of these distributions. The absorption effects lead to a large reduction of the cross section. We can see a large damping of the cross section in the region of $\phi_{pp} \sim \pi$. The ratio of full (in-

cluding absorption) and Born cross sections $\langle S^2 \rangle$, the gap survival factor, for the WA102 kinematics ($\sqrt{s} = 29.1$ GeV and $|x_{F,K^*\bar{K}^*}| \leq 0.2$) is $\langle S^2 \rangle \cong 0.4$ for the continuum contribution and 0.38 for the f_2 contribution.

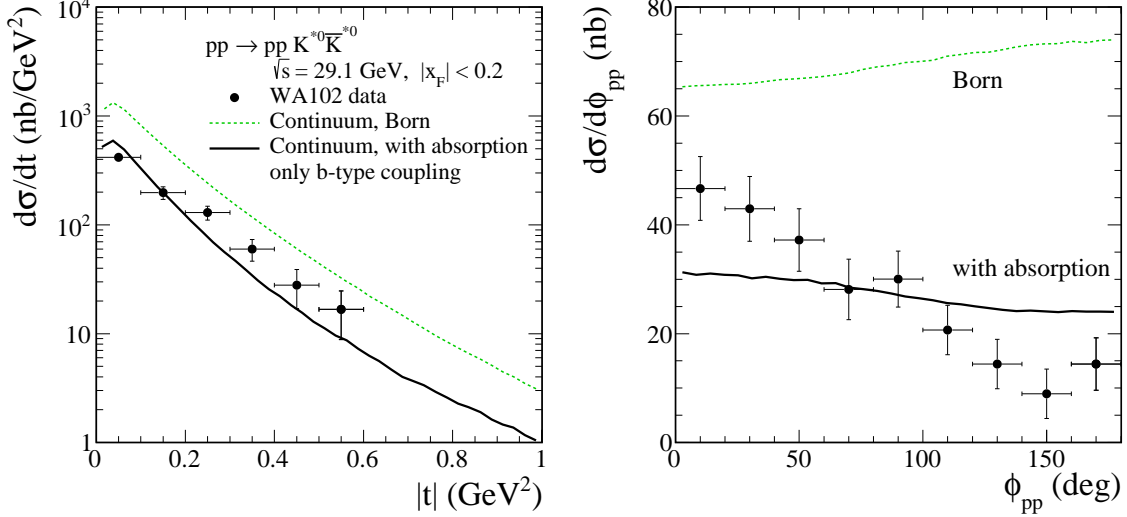


FIG. 6: The $|t|$ (left panel) and ϕ_{pp} (right panel) distributions for the $pp \rightarrow ppK^{*0}\bar{K}^{*0}$ reaction at $\sqrt{s} = 29.1$ GeV and $|x_{F,K^*\bar{K}^*}| \leq 0.2$. The data points from [10] have been normalised to the total cross section $\sigma_{\text{exp}} = 85$ nb. We show results for the continuum contribution obtained with the b -type coupling only in the Born approximation and with absorption.

In [10] also the dP_t dependence for the $K^*\bar{K}^*$ system was presented. Here, dP_t (the so-called “glueball-filter variable” [22, 51]) is defined as

$$dP_t = q_{t,1} - q_{t,2} = p_{t,2} - p_{t,1}, \quad dP_t = |dP_t|. \quad (3.1)$$

In Table I we show the WA102 experimental values for the fraction of $K^*\bar{K}^*$ production in three dP_t intervals and for the ratio of production at small dP_t to large dP_t and our corresponding results for the $f_2(1950)$ meson and continuum contributions. The calculations have been done with the absorption effects included. From the comparison to the WA102 results we see that smaller values of the cutoff parameter, $\tilde{\Lambda}_0^2 = 0.5$ GeV² in (2.18) and $\Lambda_0^2 = 0.5$ GeV² in (2.30), are preferred. We can conclude that both the continuum contribution with the b -type $\mathbb{P}K^*K^*$ coupling and the f_2 contribution with the $g^{(1)}$ and g'' couplings have similar characteristics as the WA102 data.

By comparing the theoretical results and the differential cross sections obtained by the WA102 Collaboration we fixed the parameters of our model. With them we will provide our predictions for the LHC. For the continuum term we take $|b_{\mathbb{P}K^*K^*}| = 4.37$ GeV⁻¹, $a_{\mathbb{P}K^*K^*} = 0$, $\Lambda_{\text{off},E} = 1.6$ GeV, $\Lambda_0^2 = 0.5$ GeV², and for the $f_2(1950)$ term we take $|g_{\mathbb{P}f_2}^{(1)} g_{f_2 K^*\bar{K}^*}''| = 11.0$, $\Lambda_{f_2,P} = 1.6, 2.0$ GeV, $\tilde{\Lambda}_0^2 = 0.5$ GeV².

In the future the model parameters (coupling constants, form-factor cutoff parameters) could be verified or, if necessary, adjusted by a comparison to precise experimental data from the LHC experiments.

TABLE I: Results of $K^*\bar{K}^*$ production as a function of dP_t (3.1), in three dP_t intervals, expressed as a percentage of the total contribution at the WA102 collision energy $\sqrt{s} = 29.1$ GeV and for $|x_{F,K^*\bar{K}^*}| \leq 0.2$. In the last column the ratios of $\sigma(dP_t \leq 0.2 \text{ GeV})/\sigma(dP_t \geq 0.5 \text{ GeV})$ are given. The experimental numbers are from [10]. The theoretical numbers correspond to the $f_2(1950)$ production mechanism with the $g^{(1)} \times g'$ and $g^{(1)} \times g''$ couplings, $\Lambda_{f_2,P} = 1.6$ GeV in (2.20), and $\tilde{\Lambda}_0^2 = 0.5, 1.0 \text{ GeV}^2$ in (2.18). For the continuum mechanism, we show the results only with the b -type $\mathbb{P}K^*K^*$ coupling, $\Lambda_{\text{off},E} = 1.6$ GeV in (2.31), and $\Lambda_0^2 = 0.5, 1.0 \text{ GeV}^2$ in (2.30). The absorption effects have been included in our analysis.

	$dP_t \leq 0.2 \text{ GeV}$	$0.2 \leq dP_t \leq 0.5 \text{ GeV}$	$dP_t \geq 0.5 \text{ GeV}$	Ratio
Experiment [10]	23 ± 3	54 ± 3	23 ± 2	1.00 ± 0.16
$f_2(1950), g^{(1)} \text{ and } g' \text{ couplings}$				
$\tilde{\Lambda}_0^2 = 0.5 \text{ GeV}^2$	20.9	56.3	22.8	0.92
$\tilde{\Lambda}_0^2 = 1.0 \text{ GeV}^2$	17.8	53.3	28.9	0.62
$f_2(1950), g^{(1)} \text{ and } g'' \text{ couplings}$				
$\tilde{\Lambda}_0^2 = 0.5 \text{ GeV}^2$	20.8	56.2	23.0	0.91
$\tilde{\Lambda}_0^2 = 1.0 \text{ GeV}^2$	17.7	53.1	29.2	0.61
Continuum, b -type coupling				
$\Lambda_0^2 = 0.5 \text{ GeV}^2$	20.3	55.2	24.5	0.83
$\Lambda_0^2 = 1.0 \text{ GeV}^2$	17.1	51.8	31.0	0.55

B. Predictions for the LHC experiments

Here we shall give our predictions for the reaction $pp \rightarrow ppK^+\pi^-\pi^+\pi^-$ represented by the diagrams in Fig. 1. The results were obtained in the calculations with the tensor-pomeron exchanges including the absorptive corrections within the one-channel-eikonal approach.

In Fig. 7 we present the $K^+\pi^-\pi^+\pi^-$ invariant mass distributions for the continuum K^{*0} -exchange contribution and the $f_2(1950)$ -exchange contribution for the parameters fixed by the WA102 data. According to the same strategy as in the previous section both contributions are considered separately, i.e. without possible interference effects between the continuum $K^{*0}\bar{K}^{*0}$ and the signal $f_2 \rightarrow K^{*0}\bar{K}^{*0}$ processes. The calculations were done for $\sqrt{s} = 13$ TeV with typical experimental cuts on η_M (pseudorapidities) and $p_{t,M}$ (transverse momenta) of centrally produced pions and kaons. There are shown the results with an extra cut on momenta of leading protons $0.17 \text{ GeV} < |p_{y,p}| < 0.50 \text{ GeV}$ that will be applied when using the ALFA subdetector on both sides of the ATLAS detector. We show results for larger (forward) pseudorapidities and without a measurement of outgoing protons relevant for the LHCb experiment. We can see that the distributions of both considered mechanisms have maximum around $M_{K^+K^-\pi^+\pi^-} \simeq 2 \text{ GeV}$; therefore, the continuum term close to the threshold may be misidentified as a broad $f_2(1950)$ resonance. A clear difference is visible at higher values of the invariant mass of the $K^+K^-\pi^+\pi^-$ system. The invariant mass distributions for the continuum contribution is broader compared to the $f_2(1950)$ contribution which we show for two cutoff parameters $\Lambda_{f_2,P} = 1.6 \text{ GeV}$ and 2.0 GeV . For the continuum term we show results with the K^* Regge trajectory both for the linear form (2.33) (see the lower solid lines) and the “square-root” form (2.34) (see the upper solid lines).

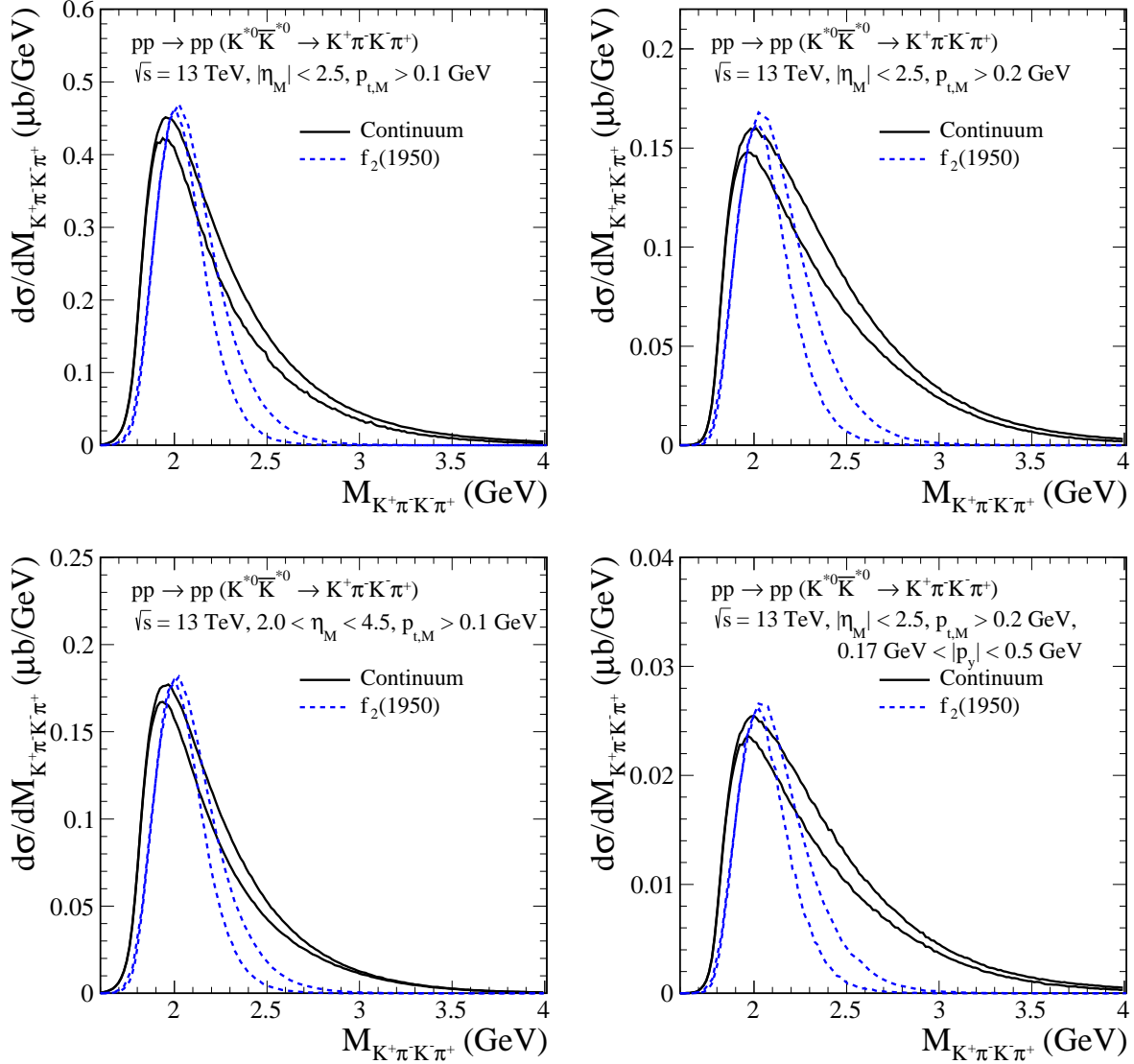


FIG. 7: Invariant mass distributions for the central $K^+\pi^-K^-\pi^+$ system via the $K^{*0}\bar{K}^{*0}$ states calculated for $\sqrt{s} = 13$ TeV with the kinematical cuts specified in the figure legends. The results for the two mechanisms are presented. For the $f_2(1950)$ term we show the results for $\Lambda_{f_2,P} = 1.6$ GeV (the lower dashed lines) and 2.0 GeV (the upper dashed lines). For the continuum term we show results for two parametrisations of the K^* Regge trajectory: the linear form (2.33) (see the lower solid lines) and the “square-root” form (2.34) (see the upper solid lines). The absorption effects are included.

In Table II we have collected integrated cross sections in nb for different experimental cuts for the exclusive $K^+K^-\pi^+\pi^-$ production via the intermediate $K^{*0}\bar{K}^{*0}$ states including the contributions shown in Fig. 1. The ratio of the full and Born cross sections at $\sqrt{s} = 13$ TeV is approximately $\langle S^2 \rangle \cong 0.19$ for the K^{*0} -exchange continuum contribution and $\langle S^2 \rangle \cong 0.18$ for the $f_2(1950)$ -exchange contribution. For the continuum, we used (2.33). For the f_2 case we show the results for $\Lambda_{f_2,P} = 1.6$ GeV (smaller cross sections) and 2.0 GeV (larger cross sections).

TABLE II: The integrated cross sections in nb for the reaction $pp \rightarrow pp(K^{*0}\bar{K}^{*0} \rightarrow K^+\pi^-K^-\pi^+)$ for the $f_2(1950)$ contribution (for $\Lambda_{f_2,P} = 1.6 - 2.0$ GeV) and the K^{*0} -exchange continuum contribution; see Fig. 1. The results have been calculated for $\sqrt{s} = 13$ TeV and some typical experimental cuts on pseudorapidities and transverse momenta of produced pions and kaons. The absorption effects were included here.

\sqrt{s} (TeV)	Cuts	Cross sections (nb)	
		$f_2(1950)$	Continuum
13	$ \eta_M < 1.0, p_{t,M} > 0.1$ GeV	18.6 – 23.7	32.1
13	$ \eta_M < 2.5, p_{t,M} > 0.1$ GeV	151.5 – 190.0	249.4
13	$ \eta_M < 2.5, p_{t,M} > 0.2$ GeV	56.5 – 75.0	109.2
13	$ \eta_M < 2.5, p_{t,M} > 0.2$ GeV, $0.17 \text{ GeV} < p_y < 0.5$ GeV	8.8 – 11.7	17.0
13	$2 < \eta_M < 4.5, p_{t,M} > 0.1$ GeV	58.6 – 72.9	93.1
13	$2 < \eta_M < 4.5, p_{t,M} > 0.2$ GeV	23.3 – 30.6	43.1

Let us complete our analysis with the following remark. We are assuming that the reaction $pp \rightarrow ppK^{*0}\bar{K}^{*0}$ is dominated by pomeron exchange, for both the $f_2(1950)$ and continuum mechanisms, already at $\sqrt{s} = 29.1$ GeV. Using this we have fixed some parameters of our model and then have calculated the cross sections for the LHC. But, the subleading reggeon-exchange contributions (e.g., $f_{2R}f_{2R^-}$, $f_{2R}\mathbb{P}^-$, $\mathbb{P}f_{2R}$ -fusion processes) can also participate. The inclusion of these subleading exchanges would introduce many new coupling parameters and form factors and would make a meaningful analysis of the WA102 data practically impossible. However, for the analysis of data from the COMPASS experiment, which operates in the same energy range as previously the WA102 experiment, it could be very worthwhile to study all the above subleading exchanges in detail. Keep in mind that at high energies and in the midrapidity region the subleading exchanges should give small contributions. However, they may influence the absolute normalization of the cross section at low energies. In general, our two mechanisms may have different production modes, and therefore also different energy dependence of the cross section. Therefore, our predictions for the LHC experiments should be regarded rather as an upper limit.

IV. CONCLUSIONS

In this paper, we have discussed diffractive production of $K^{*0}\bar{K}^{*0}$ system in proton-proton collisions within the tensor-pomeron approach. Two different mechanism have been considered, central exclusive production of the $f_2(1950)$ resonance and the continuum with the intermediate K^{*0} -meson exchange. By comparing the theoretical results and the WA102 experimental data [10] we have fixed some coupling parameters and off-shell dependencies of an intermediate mesons.

We have shown that the continuum contribution alone, taking into account the dominance of the b -type of the $\mathbb{P}K^*K^*$ coupling, describes the invariant mass spectrum obtained by the WA102 Collaboration reasonably well. This is not the case for the $f_2(1950)$ meson for which an agreement with the WA102 data for the preferred type of couplings $g_{\mathbb{P}\mathbb{P}f_2}^{(1)}$ and $g_{f_2K^*\bar{K}^*}''$ in the limited invariant mass range was found. We have found that, in both cases, the model results are in better agreement with the WA102 data taking into

account the tensor-vector-vector vertices (couplings) with the $\Gamma^{(2)}$ function rather than $\Gamma^{(0)}$ one. This observation in our tensor-pomeron approach should be verified by future experimental results. Hopefully this will be the case at the LHC.

In the calculation the absorptive corrections calculated at the amplitude level and related to the proton-proton nonperturbative interactions have been included. It is known that the absorption effects considerably change the shape of the distribution for ϕ_{pp} , the azimuthal angle between the outgoing protons, and the shape of the distribution for dP_t , the difference of the transverse momentum vectors of the outgoing protons. The ϕ_{pp} and dP_t dependences for the $K^{*0}\bar{K}^{*0}$ system was measured by the WA102 Collaboration. We have reproduced these results fairly well in our model including absorption effects. The final distributions in these variables for both mechanisms considered are very similar to each other.

Assuming that the WA102 data are already dominated by pomeron exchange, we have calculated the cross sections for the reaction $pp \rightarrow ppK^{*0}\bar{K}^{*0}$ for experiments at the LHC imposing cuts on pseudorapidities and transverse momenta of the pions and kaons from the decays $K^{*0}\bar{K}^{*0} \rightarrow (K^+\pi^-)(K^-\pi^+)$. The distributions of the invariant mass of the $K^+\pi^-K^-\pi^+$ system have been presented. We should keep in mind that both considered mechanisms have a maximum around $M_{K^+K^-\pi^+\pi^-} \simeq 2$ GeV, thus a broad enhancement (at least part of it) in this mass region can be misidentified as the $f_2(1950)$ resonance. Furthermore, a similar behaviour of the continuum and f_2 production processes makes an identification of a hypothetical tensor-glueball state in this reaction rather difficult.

We have found in this paper that the diffractive processes leads to a cross section for the $K^{*0}\bar{K}^{*0} \rightarrow K^+\pi^-K^-\pi^+$ production more than one order of magnitude larger than the corresponding cross section for the $\phi(1020)\phi(1020) \rightarrow K^+K^-K^+K^-$ processes considered in [41]. Our predictions can be tested by all collaborations (ALICE, ATLAS, CMS, LHCb) working at the LHC. A measurable cross section for the exclusive process $pp \rightarrow pp(K^{*0}\bar{K}^{*0} \rightarrow K^+\pi^-K^-\pi^+)$ should provide an interesting challenge to check and explore.

Acknowledgments

I am indebted to Antoni Szczurek and Otto Nachtmann for useful discussions. This work was partially supported by the Polish National Science Centre under Grant No. 2018/31/B/ST2/03537.

-
- [1] H. Albrecht *et al.*, (ARGUS Collaboration), *First observation of $\gamma\gamma \rightarrow K^{*0}\bar{K}^{*0}$* , Phys. Lett. **B198** (1987) 255.
 - [2] H. Albrecht *et al.*, (ARGUS Collaboration), *First observation of $\gamma\gamma \rightarrow K^{*+}K^{*-}$* , Phys. Lett. **B212** (1988) 528.
 - [3] H. Albrecht *et al.*, (ARGUS Collaboration), *Measurement of $K^*\bar{K}^*$ production in two-photon interactions*, Eur. Phys. J. **C16** (2000) 435.
 - [4] U. Mallik, (MARKIII Collaboration), *Results From Mark-III On The J/ψ Decays*, AIP Conf. Proc. **185** (1989) 325.
 - [5] G. Eigen, (MARKIII Collaboration), *Study of $K^{*0}\bar{K}^{*0}$ production in radiative J/ψ decays*, Nucl. Phys. Proc. Suppl. **21** (1991) 149.

- [6] D. Aston *et al.*, Strangeonia and Kin: New Results from Kaon Hadroproduction with LASS, in *Hadron '89. Proceedings, 3rd International Conference on Hadron Spectroscopy, Ajaccio, France, September 23-27, 1989.*
<https://slac.stanford.edu/pubs/slacpubs/5000/slac-pub-5150.pdf>.
- [7] D. Aston *et al.*, *Strangeonium production from LASS*, Nucl. Phys. Proc. Suppl. **21** (1991) 5.
- [8] T. A. Armstrong *et al.*, (WA76 Collaboration), *Study of the $K^+K^-\pi^+\pi^-$ system centrally produced in the reactions $\pi^+p \rightarrow \pi^+(K^+K^-\pi^+\pi^-)p$ and $pp \rightarrow p(K^+K^-\pi^+\pi^-)p$ at 85 GeV/c*, Z. Phys. **C34** (1987) 33.
- [9] T. A. Armstrong *et al.*, (WA76 Collaboration), *A study of the centrally produced $K^{*0}\bar{K}^{*0}$ final state in the reaction $pp \rightarrow p_f(K^+K^-\pi^+\pi^-)p_s$ at 300 GeV/c*, Z. Phys. **C46** (1990) 405.
- [10] D. Barberis *et al.*, (WA102 Collaboration), *A study of the centrally produced $K^*(892)$ anti- $K^*(892)$ and $\phi\omega$ systems in pp interactions at 450 GeV/c*, Phys. Lett. **B436** (1998) 204, arXiv:hep-ex/9807021 [hep-ex].
- [11] D. Barberis *et al.*, (WA102 Collaboration), *A study of the centrally produced $\phi\phi$ system in pp interactions at 450 GeV/c*, Phys. Lett. **B432** (1998) 436, arXiv:hep-ex/9805018 [hep-ex].
- [12] A. Breakstone *et al.*, (ABCDHW Collaboration), *Inclusive Pomeron-Pomeron interactions at the CERN ISR*, Z.Phys. **C42** (1989) 387.
- [13] D. Barberis *et al.*, (WA102 Collaboration), *A study of the $f_0(1370)$, $f_0(1500)$, $f_0(2000)$ and $f_2(1950)$ observed in the centrally produced 4π final states*, Phys.Lett. **B474** (2000) 423, arXiv:0001017 [hep-ex].
- [14] F. Br  nner, D. Parganlija, and A. Rebhan, *Glueball decay rates in the Witten-Sakai-Sugimoto model*, Phys. Rev. D **91** no. 10, (2015) 106002, arXiv:1501.07906 [hep-ph]. [Erratum: Phys. Rev. D **93** (2016) 109903].
- [15] A. A. Godizov, *The ground state of the Pomeron and its decays to light mesons and photons*, Eur. Phys. J. C **76** no. 7, (2016) 361, arXiv:1604.01689 [hep-ph].
- [16] P. Zhang, L.-P. Zou, and Y. M. Cho, *Abelian decomposition and glueball-quarkonium mixing in QCD*, Phys. Rev. D **98** no. 9, (2018) 096015, arXiv:1606.02374 [hep-ph].
- [17] C. J. Morningstar and M. J. Peardon, *Glueball spectrum from an anisotropic lattice study*, Phys.Rev. **D60** (1999) 034509, arXiv:hep-lat/9901004 [hep-lat].
- [18] E. Gregory, A. Irving, B. Lucini, C. McNeile, A. Rago, C. Richards, and E. Rinaldi, *Towards the glueball spectrum from unquenched lattice QCD*, JHEP **10** (2012) 170, arXiv:1208.1858 [hep-lat].
- [19] W. Sun, L.-C. Gui, Y. Chen, M. Gong, C. Liu, Y.-B. Liu, Z. Liu, J.-P. Ma, and J.-B. Zhang, *Glueball spectrum from $N_f = 2$ lattice QCD study on anisotropic lattices*, Chin. Phys. **C42** no. 9, (2018) 093103, arXiv:1702.08174 [hep-lat].
- [20] I. Szanyi, L. Jenkovszky, R. Schicker, and V. Svintozelskyi, *Pomeron/glueball and odderon/oddball trajectories*, Nucl. Phys. A **998** (2020) 121728, arXiv:1910.02494 [hep-ph].
- [21] A. Kirk, *Resonance production in central pp collisions at the CERN Omega spectrometer*, Phys.Lett. **B489** (2000) 29, arXiv:0008053 [hep-ph].
- [22] F. E. Close and A. Kirk, *Glueball - $q\bar{q}$ filter in central hadron production*, Phys.Lett. **B397** (1997) 333, arXiv:hep-ph/9701222 [hep-ph].
- [23] K. Abe *et al.*, (Belle Collaboration), *Measurement of K^+K^- production in two-photon collisions in the resonant-mass region*, Eur. Phys. J. C **32** (2003) 323, arXiv:hep-ex/0309077.
- [24] S. Uehara *et al.*, (Belle Collaboration), *High-statistics study of neutral-pion pair production in two-photon collisions*, Phys. Rev. D **79** (2009) 052009, arXiv:0903.3697 [hep-ex].
- [25] M. K  usek-Gawenda, P. Lebiedowicz, O. Nachtmann, and A. Szczurek, *From the $\gamma\gamma \rightarrow p\bar{p}$*

- reaction to the production of $p\bar{p}$ pairs in ultraperipheral ultrarelativistic heavy-ion collisions at the LHC, Phys. Rev. D **96** no. 9, (2017) 094029, arXiv:1708.09836 [hep-ph].
- [26] C. Ewerz, M. Maniatis, and O. Nachtmann, *A Model for Soft High-Energy Scattering: Tensor Pomeron and Vector Odderon*, Annals Phys. **342** (2014) 31–77, arXiv:1309.3478 [hep-ph].
 - [27] D. Ebert, R. N. Faustov, and V. O. Galkin, *Masses of light tetraquarks and scalar mesons in the relativistic quark model*, Eur. Phys. J. C **60** (2009) 273, arXiv:0812.2116 [hep-ph].
 - [28] Q.-F. Lü, K.-L. Wang, and Y.-B. Dong, *The $ss\bar{s}\bar{s}$ tetraquark states and the newly observed structure $X(2239)$ by BESIII Collaboration*, Chin. Phys. C **44** no. 2, (2020) 024101, arXiv:1903.05007 [hep-ph].
 - [29] P. Zyla *et al.*, (Particle Data Group), *Review of Particle Physics*, PTEP **2020** no. 8, (2020) 083C01.
 - [30] F.-X. Liu, M.-S. Liu, X.-H. Zhong, and Q. Zhao, *Fully-strange tetraquark $ss\bar{s}\bar{s}$ spectrum and possible experimental evidence*, arXiv:2008.01372 [hep-ph].
 - [31] H. Kim, K. S. Kim, M.-K. Cheoun, D. Jido, and M. Oka, *Further signatures to support the tetraquark mixing framework for the two light-meson nonets*, Phys. Rev. D **99** no. 1, (2019) 014005, arXiv:1811.00187 [hep-ph].
 - [32] O. Nachtmann, *Considerations concerning diffraction scattering in quantum chromodynamics*, Annals Phys. **209** (1991) 436–478.
 - [33] P. Lebiedowicz, O. Nachtmann, and A. Szczurek, *Exclusive central diffractive production of scalar and pseudoscalar mesons; tensorial vs. vectorial pomeron*, Annals Phys. **344** (2014) 301–339, arXiv:1309.3913 [hep-ph].
 - [34] P. Lebiedowicz, O. Nachtmann, and A. Szczurek, ρ^0 and Drell-Söding contributions to central exclusive production of $\pi^+\pi^-$ pairs in proton-proton collisions at high energies, Phys. Rev. D **91** (2015) 074023, arXiv:1412.3677 [hep-ph].
 - [35] P. Lebiedowicz, O. Nachtmann, and A. Szczurek, *Central exclusive diffractive production of the $\pi^+\pi^-$ continuum, scalar and tensor resonances in pp and $p\bar{p}$ scattering within the tensor Pomeron approach*, Phys. Rev. D **93** (2016) 054015, arXiv:1601.04537 [hep-ph].
 - [36] P. Lebiedowicz, O. Nachtmann, and A. Szczurek, *Extracting the pomeron-pomeron- $f_2(1270)$ coupling in the $pp \rightarrow pp\pi^+\pi^-$ reaction through angular distributions of the pions*, Phys. Rev. D **101** no. 3, (2020) 034008, arXiv:1901.07788 [hep-ph].
 - [37] P. Lebiedowicz, O. Nachtmann, and A. Szczurek, *Central production of ρ^0 in pp collisions with single proton diffractive dissociation at the LHC*, Phys. Rev. D **95** no. 3, (2017) 034036, arXiv:1612.06294 [hep-ph].
 - [38] P. Lebiedowicz, O. Nachtmann, and A. Szczurek, *Towards a complete study of central exclusive production of K^+K^- pairs in proton-proton collisions within the tensor Pomeron approach*, Phys. Rev. D **98** (2018) 014001, arXiv:1804.04706 [hep-ph].
 - [39] P. Lebiedowicz, O. Nachtmann, and A. Szczurek, *Exclusive diffractive production of $\pi^+\pi^-\pi^+\pi^-$ via the intermediate $\sigma\sigma$ and $\rho\rho$ states in proton-proton collisions within tensor pomeron approach*, Phys. Rev. D **94** no. 3, (2016) 034017, arXiv:1606.05126 [hep-ph].
 - [40] P. Lebiedowicz, O. Nachtmann, and A. Szczurek, *Central exclusive diffractive production of $p\bar{p}$ pairs in proton-proton collisions at high energies*, Phys. Rev. D **97** no. 9, (2018) 094027, arXiv:1801.03902 [hep-ph].
 - [41] P. Lebiedowicz, O. Nachtmann, and A. Szczurek, *Central exclusive diffractive production of $K^+K^-K^+K^-$ via the intermediate $\phi\phi$ state in proton-proton collisions*, Phys. Rev. D **99** no. 9, (2019) 094034, arXiv:1901.11490 [hep-ph].
 - [42] P. Lebiedowicz, O. Nachtmann, and A. Szczurek, *Searching for the odderon in $pp \rightarrow ppK^+K^-$ and $pp \rightarrow pp\mu^+\mu^-$ reactions in the $\phi(1020)$ resonance region at the LHC*,

- Phys. Rev. D **101** no. 9, (2020) 094012, arXiv:1911.01909 [hep-ph].
- [43] P. Lebiedowicz, J. Leutgeb, O. Nachtmann, A. Rebhan, and A. Szczurek, *Central exclusive diffractive production of axial-vector $f_1(1285)$ and $f_1(1420)$ mesons in proton-proton collisions*, Phys. Rev. D **102** no. 11, (2020) 114003, arXiv:2008.07452 [hep-ph].
 - [44] R. Sikora, *Measurement of the diffractive central exclusive production in the STAR experiment at RHIC and the ATLAS experiment at LHC*. PhD thesis, AGH University of Science and Technology, Cracow, Sep, 2020. <https://cds.cern.ch/record/2747846>.
 - [45] A. Donnachie and P. V. Landshoff, *Total cross sections*, Phys.Lett. **B296** (1992) 227–232, arXiv:hep-ph/9209205 [hep-ph].
 - [46] A. Donnachie, H. G. Dosch, P. V. Landshoff, and O. Nachtmann, *Pomeron physics and QCD*, Camb.Monogr.Part.Phys.Nucl.Phys.Cosmol. **19** (2002) 1–347.
 - [47] D. Melikhov, O. Nachtmann, V. Nikonov, and T. Paulus, *Masses and couplings of vector mesons from the pion electromagnetic, weak, and $\pi\gamma$ transition form factors*, HD-THEP-03-58, Eur.Phys.J. **C34** (2004) 345–360, arXiv:hep-ph/0311213 [hep-ph].
 - [48] L. A. Harland-Lang, V. A. Khoze, and M. G. Ryskin, *Modelling exclusive meson pair production at hadron colliders*, Eur.Phys.J. **C74** (2014) 2848, arXiv:1312.4553 [hep-ph].
 - [49] P. D. B. Collins, *An introduction to Regge theory and high energy physics*. Cambridge University Press, 1977.
 - [50] M. M. Brisudová, L. Burakovsky, and J. T. Goldman, *Effective functional form of Regge trajectories*, Phys. Rev. D **61** (2000) 054013, arXiv:hep-ph/9906293.
 - [51] D. Barberis *et al.*, (WA102 Collaboration), *A kinematical selection of glueball candidates in central production*, Phys.Lett. **B397** (1997) 339.